Chapter in **Advancing Astrophysics with the SKA – II**

The SKA View of Cool-core Clusters: Evolution of Radio Mini-halos and AGN Feedback

Myriam Gitti[1,2] Paolo Tozzi[3] Francesco Ubertosi[1,2] Annalisa Bonafede[1,2] Gianfranco Brunetti[2] Rossella Cassano[2] Stefano Ettori[4,5] Luigina Feretti[2] Marie-Lou Gendron-Marsolais[6] Simona Giacintucci[7] Julie Hlavacek-Larrondo[8] Alessandro Ignesti[9] Giulia Macario[3,10] Mamta Pandey-Pommier[11] and Tiziana Venturi[2]

[1]*Dipartimento di Fisica e Astronomia, Università di Bologna, via Gobetti 93/2, 40129 Bologna, Italy*
[2]*INAF – Istituto di Radioastronomia, via Gobetti 101, 40129 Bologna, Italy*
[3]*INAF – Osservatorio Astrofisico di Arcetri, Largo Enrico Fermi 5, 50125 Firenze, Italy*
[4]*INAF – Osservatorio di Astrofisica e Scienza dello Spazio, via Gobetti 93/3, 40129 Bologna, Italy*
[5]*INFN – Sezione di Bologna, viale Berti Pichat 6/2, 40127 Bologna, Italy*
[6]*Dép. de physique, de génie physique et d'optique, Université Laval, Québec (QC), G1V 0A6, Canada*
[7]*Naval Research Laboratory, 4555 Overlook Avenue SW, Code 7213, Washington, DC 20375, USA*
[8]*Département de physique, Physics department, Université de Montréal*
[9]*INAF – Astronomical Observatory of Padova, vicolo dell'Osservatorio 5, IT-35122 Padova, Italy*
[10]*SKAO, SKA-Low Science Operations Centre, 26 Dick Perry Avenue, Kensington WA 6151, Australia*
[11]*Pole Scientific, University Catholic of Lyon- University of Lyon, 10 place des Archives 69288, Lyon, France*

E-mail: myriam.gitti@unibo.it

In about 70% of relaxed, cool-core galaxy clusters, the brightest cluster galaxy (BCG) is radio loud, showing non-thermal radio jets and lobes ejected by the central active galactic nucleus (AGN). In recent years such relativistic plasma has been shown to interact with the surrounding thermal intra-cluster medium (ICM) as revealed by striking images where radio lobe fill the cavities in the X-ray-emitting gas. This 'radio-mode feedback' phenomenon is widespread and crucial for understanding the physics of cluster cores and the properties of the central BCG. Mechanically-powerful AGN are expected to drive turbulence in the central ICM which may also contribute to the origin of non-thermal emission on cluster-scales. Diffuse non-thermal emission has been observed in many cool-core clusters in the form of a radio mini-halo surrounding the radio-loud BCG on scales comparable to the cooling radius. Large samples of mini-halos are essential to clarify their origin and their link with the thermal and dynamical properties of clusters, especially in view of future high-resolution X-ray studies with *NewAthena* X–IFU. All-sky surveys with the SKA-Mid telescope at arcsecond resolution would have the potential to detect up to ~3500 mini-halos at redshift $z < 1$ (compared to the few tens currently known). Deep Tier surveys with the SKA-Mid at sub-arcsecond resolution would further enable a complete census of radio-loud BCGs down to 1.4 GHz powers of 10^{23} W/Hz up to $z \sim 2$. This will provide a comprehensive view of AGN feedback and its role in shaping large scale structures.

1 Introduction

The majority of baryons in galaxy clusters reside in the hot, diffuse intra-cluster medium (ICM), mostly heated by gravitational processes to 1-10 keV and observable via thermal bremsstrahlung and line emission in X-rays. Yet, the expected catastrophic cooling and the consequent formation of adiabatic cooling flows in relaxed cluster cores (Fabian, 1994) is not observed (e.g., Peterson and Fabian, 2006), implying that non-gravitational heating processes act on ∼100 kpc scales around the brightest cluster galaxy (BCG). Understanding the interaction between gravitational physics, relativistic plasma injected by the active galactic nucleus (AGN), and the ICM is key to tracing galaxy growth, star formation history, and large-scale structure assembly. In particular, AGN feedback has emerged as a fundamental component of galaxy evolution models, with its clearest manifestation in *cool-core* (CC) clusters – systems with short central cooling times, high densities ($n_e > 10^{-2}$ cm^{-3}), and relatively low temperatures ($kT <$ few keV). Although the presence of ICM at temperatures below ∼1 keV, as predicted by the classical adiabatic cooling-flow model, is generally not observed (e.g., Peterson and Fabian, 2006) except in a few rare cases (Pinto et al., 2018), the strength of the cool core has nonetheless been shown to correlate with both the star formation rate and the nuclear accretion rate, suggesting that systems with the strongest cool cores host cooling processes (McDonald et al., 2018). Therefore, CC clusters are ideal laboratories for studying AGN–ICM interactions.

BCGs in CC clusters often host FR-I radio sources (Fanaroff and Riley, 1974), detected in ∼70% of cases (Burns, 1990; Dunn and Fabian, 2006; Best et al., 2007; Mittal et al., 2009). *Chandra* and *XMM-Newton* observations reveal that the X-ray-emitting gas is displaced by radio jets, which inflate lobes (radio *bubbles*) and create *cavities* visible as depressions in the X-ray surface brightness. Striking composite images, where radio lobes precisely fill X-ray cavities, establish radio galaxies as a primary source of feedback able to mitigate and possibly solve the cooling flow problem (e.g., McNamara and Nulsen, 2007; Gitti et al., 2012; Fabian, 2012; Gaspari et al., 2013; Donahue and Voit, 2022). The mechanisms by which AGN jets heat the ICM likely involve buoyant bubbles, shocks, and turbulence (e.g., Eckert et al., 2021). AGN-inflated bubbles may dissipate enthalpy as they rise through the ICM (McNamara and Nulsen, 2007, 2012), and are observed in roughly 50% of mass-selected and 60-90% of X-ray-selected CCs (Olivares et al., 2022; Fabian, 2012). Jets can also drive shocks (e.g., Heinz and Churazov, 2005), which may offer a more direct and isotropic energy transfer (Nulsen and McNamara, 2013; Ubertosi et al., 2023). However, due to observational limits, to date fewer than twenty systems show clear detections of shocks (e.g., Ubertosi et al., 2023). A third mechanism is AGN-driven turbulence, which may both heat the ICM (e.g., Zhuravleva et al., 2014) and re-accelerate relativistic particles (Bravi et al., 2016), possibly seeded by disrupted AGN bubbles.

Diffuse non-thermal radio emission is indeed observed in a few tens of CC clusters as *radio mini-halos*, surrounding the BCG. These faint, steep-spectrum ($\alpha > 1$, where the flux density at the frequency ν is $S_\nu \propto \nu^{-\alpha}$) sources extend over ∼100-500 kpc and have typical 1.4 GHz powers of $\sim 10^{23}$-10^{24} W/Hz (e.g., Feretti et al., 2012; van Weeren et al., 2019). Unlike bubbles, mini-halos originate from the ICM itself, where thermal plasma and relativistic electrons mix. Figure 1 shows a clear example of radio lobes (white contours), filling X-ray cavities, which are distinct from the mini-halo (green contours). Mini-halos trace ∼GeV electrons in ∼μG magnetic fields, similar to

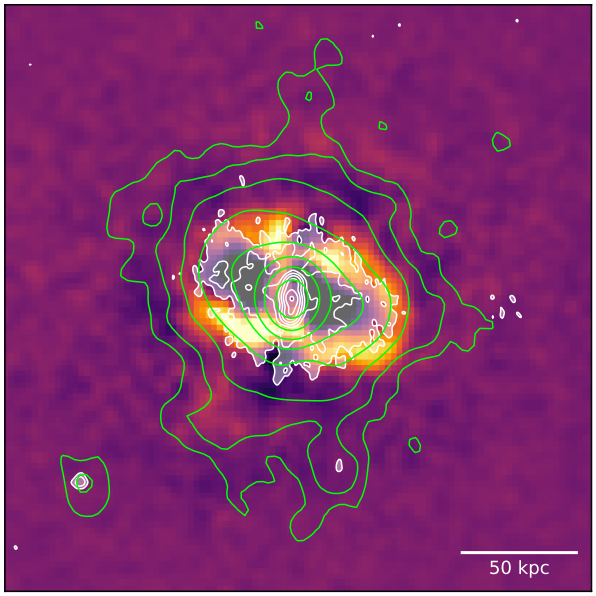

Figure 1: The X-ray *Chandra* image (residual after β-model subtraction) of the galaxy cluster RBS 797 at $z = 0.35$ (Ubertosi et al., 2021) is shown in color scale with superimposed VLA contours at 1.4 GHz (green, Gitti et al., 2006) and at 3 GHz (white, Ubertosi et al., 2024a). Contours levels start at 3×rms (rms ∼13 μJy/beam at 1.4 GHz and 5 μJy/beam at 3 GHz; beam ∼ 3″ at 1.4 GHz and 0.9″ at 3 GHz), and increase by a factor of 2. The X-ray cavities, visible as depressions in the X-ray surface brightness, are filled with the BCG radio lobes (white contours), that have also driven cocoon shock fronts in the ICM (Ubertosi et al., 2023); on larger scale, a radio mini-halo is detected (green contours).

giant halos. However, while giant halos (which extend on $\gtrsim$ Mpc-scale) are merger-driven and found in non-CC clusters (see e.g., Cassano et al., 2026), mini-halos are detected in relaxed CC systems and are likely linked to AGN activity, though not directly powered by it. Electrons may be injected by the AGN and re-accelerated by turbulence in the core, possibly driven by the AGN itself (e.g., Richard-Laferrière et al., 2020) or gas sloshing (e.g., Mazzotta and Giacintucci, 2008). This suggests that mechanisms less extreme than mergers, as AGN feedback and sloshing are, can sustain non-thermal emission (note however that while radio emission is always associated with the BCG in CC clusters, AGN feedback and sloshing are not ubiquitous, e.g., Giacintucci et al. (2019) and references therein), though the exact process remains uncertain (see Sect. 2.1).

Cool cores are already established at $z \sim 1$ (Santos et al., 2012), and are consistently associated with both radio-loud AGN and mini-halos (Sun, 2009; Feretti et al., 2012). However, current systematic studies of AGN feedback and mini-halos are mostly limited to $z < 0.7$ (Hlavacek-Larrondo et al., 2012)[1], despite ICM in cluster halos is being detected up to $z \gtrsim 1.6$ (e.g., Tozzi et al., 2015; Mantz et al., 2020; Hlavacek-Larrondo et al., 2020; Andreon et al., 2023; Lepore et al., 2024). A mild negative evolution of mini-halos with redshift may be associated to the decrease of CC clusters in favor of a population of mergers or dynamically unrelaxed clusters (Santos et al., 2010; McDonald et al., 2013). However, the current gap is mainly due to observational challenges: mini-halos must be disentangled from the bright central AGN emission, which can reach few Jy/arcsec^2 at 1.4 GHz (as e.g., in Perseus), while the typical mini-halo brightness is only a few μJy/arcsec^2. This requires high sensitivity, dynamic range, and sub-arcsec to milliarcsec angular resolution — capabilities uniquely offered by the Square Kilometre Array Observatory[2] (SKAO, Braun et al., 2019).

Studying non-thermal activity and radio-mode feedback is essential for understanding ICM physics and cosmic structure evolution. The SKAO will play a unique and game-changing role in tracing

[1] One mini-halo candidate was recently identified at $z \sim 1.7$ (Hlavacek-Larrondo et al., 2025).

[2] https://www.skao.int/en/science-users/118/ska-telescope-specifications

non-thermal emission associated to mini-halos and AGN feedback in cluster cores up to the highest redshifts. In this chapter, we focus on insights into radio mini-halos (Sect. 2) and AGN feedback (Sect. 3) from SKA-Mid statistical studies, updating the work presented in Gitti et al. (2015) and highlighting the strong synergy with future X-ray missions. Potential contributions from SKA-Low surveys are expected to be similar to those discussed in previous mini-halo studies (Gitti et al., 2018), while being less optimal for AGN feedback investigations due to the limited angular resolution, and are therefore only briefly discussed here. Our conclusions are summarized in Sect. 4. Throughout the paper, we adopt a ΛCDM cosmology with $H_0 = 70$ km s^{-1}Mpc^{-1}, $\Omega_M = 1 - \Omega_\Lambda = 0.3$.

2 Radio mini-halos

2.1 Current understanding of the mini-halo origin and open questions

Galaxy clusters hosting radio mini-halos invariably contain a central radio-loud AGN, often showing radio lobes and bubbles that inject relativistic electrons into the cluster core. While AGN may provide the primary source of relativistic particles, they cannot alone account for the diffuse emission without additional dynamical input. As with giant radio halos (see also Cassano et al., 2026), the origin of mini-halos is challenged by the short radiative lifetime of relativistic electrons compared to the size of the emission region. Two main models address this "slow-diffusion problem": in situ re-acceleration by turbulence in the cool core (Gitti et al., 2002, 2004; Mazzotta and Giacintucci, 2008; ZuHone et al., 2013), and hadronic models where secondary electrons are produced via p-p collisions (Pfrommer and Enßlin, 2004; Jacob and Pfrommer, 2017; Ignesti et al., 2020); see Brunetti and Jones (2014) for a review.

A key question in re-acceleration models is the origin of turbulence and its link to the central AGN. Turbulence may arise from AGN jets and lobes interacting with the ICM (e.g., Heinz et al., 2006; Zhuravleva et al., 2016). Turbulent heating has also been proposed as a mechanism for maintaining thermal balance in the ICM (Dennis and Chandran, 2005; Gaspari et al., 2012; Zhuravleva et al., 2014). If turbulence is partly dissipated into heat and partly channeled into particle re-acceleration, a shared origin for both gas heating and mini-halos is possible (Bravi et al., 2016). A decade ago, the first direct measurement of turbulence was obtained in the Perseus cluster, and it has been shown to be consistent with re-acceleration requirements (Hitomi Collaboration, 2016, 2017). With the advent of the X-Ray Imaging and Spectroscopy Mission (*XRISM*; XRISM Science Team, 2022), launched in 2023, turbulence has been measured with the spectrometer *Resolve* in a handful of nearby clusters, providing an observational basis for mini-halo models (XRISM Collaboration et al., 2025b,c,a). However, current measurements provide contradictory results on the consistency with the expected level of turbulence from hydrodynamic simulations (e.g., Vazza and Brunetti, 2025). This scenario implies a close but complex link between thermal and non-thermal components, which requires to be further tested in the case of AGN-induced turbulence by examining AGN feedback in mini-halo clusters (see Sect. 3). With future generation X-ray facilities, this scenario can be investigated in greater detail with spatially resolved analysis (see Sect. 2.3). Hadronic models offer a viable alternative, where cosmic-ray instabilities heat the ICM (Fujita and Ohira, 2012; Jacob and Pfrommer, 2017). Unlike giant halos, the expected γ-ray emission from mini-halos remains consistent with current observational limits (e.g., Ahnen et al., 2016; Jacob and Pfrommer, 2017; Ignesti et al., 2020), leaving this alternative model for the origin of mini-halos substantially

unconstrained.

Another open issue is the link between mini-halos and cluster gas dynamics. Mild dynamical activity in some systems suggests that, beyond AGN feedback, minor mergers and sloshing may also inject turbulence (e.g., Gitti et al., 2007; Cassano et al., 2008; Mazzotta and Giacintucci, 2008; Riseley et al., 2022). Simulations support this view (e.g., ZuHone et al., 2013), as do spiral-shaped cold fronts in CC clusters (e.g., Markevitch and Vikhlinin, 2007), likely caused by subhalo-induced sloshing (Fujita et al., 2004; Ascasibar and Markevitch, 2006; Zuhone and Roediger, 2016). A hybrid scenario is also plausible, where AGN feedback drives most of the turbulence while sloshing mostly shapes the mini-halo morphology (Richard-Laferrière et al., 2020). Furthermore, LOFAR has recently revealed a correlation between the radial radio spectral index and AGN-driven shock fronts in one system, showing a flattening trend from the center to the edge that is unique among mini-halos and reminiscent of shock-reaccelerated particles (Bonafede et al., 2023). However, the authors show that shock re-acceleration alone cannot reproduce the observed radial brightness profile of the mini-halo. One possibility is that AGN-driven shocks propagate through a pre-existing mini-halo, re-accelerating and compressing the radio plasma and thereby producing the observed radial spectral flattening. Alternatively, in the presence of a high magnetic field (with central value $> 15\,\mu$G and a radial declining profile), turbulent re-acceleration may also account for the observed radial spectral flattening, independently of shocks. In this case, similar behaviour would be expected in all mini-halos with comparable magnetic field strengths. Deeper observations and systematic studies of other mini-halos will be required to confirm or rule out this scenario.

Some CC clusters also host large-scale radio emission in the form of giant radio halos or hybrid morphologies (e.g., Sommer et al., 2017; Savini et al., 2019; Biava et al., 2021, 2024; Riseley et al., 2022; Lusetti et al., 2024). The Perseus cluster, for example, shows filamentary substructures and a distinct large-scale radio halo (van Weeren et al., 2024). These sources suggest that minor mergers, while not energetic enough to disrupt the cool core, may still trigger particle acceleration in the ICM on scales of hundreds of kiloparsecs. A joint X-ray and radio analysis of a sample of CC clusters observed at a low frequency further indicates that cluster-scale diffuse radio emission is correlated to the presence of cold fronts (Biava et al., 2024). The co-existence of cluster-scale diffuse radio emission and cold fronts in these CC systems implies the presence of sloshing motions capable of generating sufficient turbulence to re-accelerate particles on large scales while preserving the central cool core. The large-scale halo typically shows properties that are distinct from that of the inner mini-halo, indicating that these radio phenomena may coexist in the same cluster and suggesting a possible evolutionary link (Zandanel et al., 2014; Brunetti and Jones, 2014; van Weeren et al., 2026).

Our understanding of mini-halos thus remains incomplete. Distinguishing between the leptonic and hadronic origin of mini-halos, or understanding their connection with AGN-induced turbulence and with the ICM dynamics, offers a unique probe of ICM microphysics, including magnetic field amplification and cosmic-ray transport. A breakthrough is expected from future SKA spectral and polarimetric observations, especially when combined with hard X-ray and γ-ray constraints.

2.2 Detecting radio mini-halos: radio follow-up of X-ray cluster samples

Large-sample studies will be crucial to address key questions: *(i)* Are mini-halos ubiquitous in CC clusters, and how does their occurrence evolve with redshift? *(ii)* What role does the central AGN

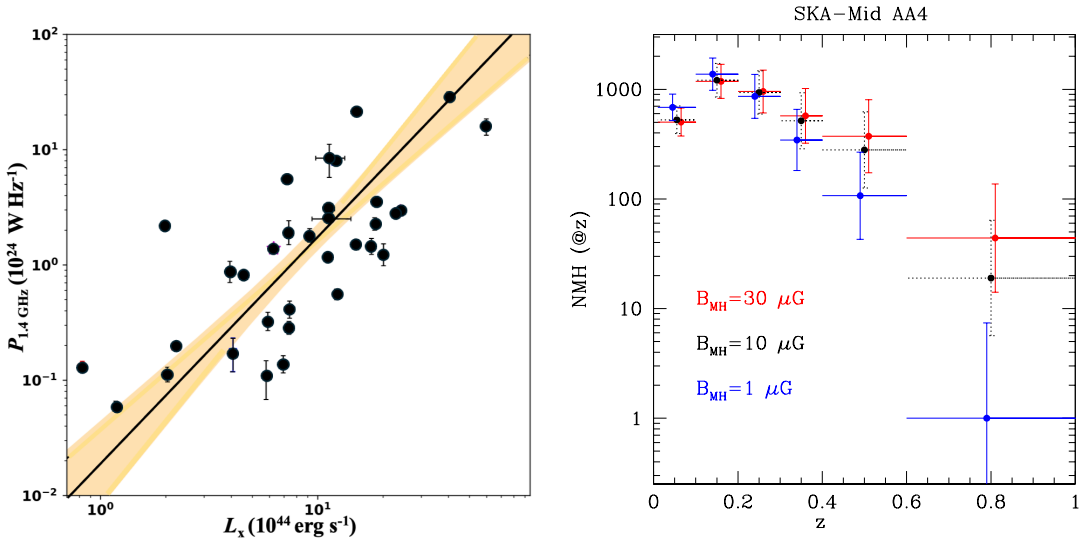

Figure 2: *Left panel:* Mini-halo radio power at 1.4 GHz versus the cluster X-ray luminosity inside a radius of 600 kpc for the mini-halo sample of Richard-Laferrière et al. (2020). The best-fitting line using the BCES-orthogonal method (Akritas and Bershady, 1996), which is calculated including also candidate and uncertain mini-halos, is displayed (black solid line) along with the 95% confidence region (orange shaded area). The best-fit values are $a = 1.97 \pm 0.31$ and $b = -1.72 \pm 0.31$ (see Eq. 1). *Right panel:* number of radio mini-halo expected in the all-sky (3π sr) survey by AA4 SKA-Mid at Band 2 (see Table 1) in different redshift bins, estimated by assuming three reference values of magnetic field strength $B_{\rm MH} = 1\,\mu$G, 10 μG, 30 μG (blue, black and red, respectively). The vertical error bars indicate the 1σ uncertainty driven by the $P_{1.4}$-$L_{\rm X}$ correlation and the horizontal bars indicate the size of the redshift bin. The points corresponding to the different $B_{\rm MH}$-field values in the same redshift bin are slightly shifted on the x-axis to improve clarity.

play, and how often is AGN feedback observed in mini-halo clusters? *(iii)* What is the origin and role of turbulence in powering mini-halos? We will show that surveys with the SKA telescopes have the capability to address these fundamental questions.

The detection of radio mini-halos is complicated by the need to separate their faint, low surface brightness emission from the bright emission of the radio-loud BCG embedded in it (see Sect. 1). This requires observations performed with a technical setup ensuring high sensitivity to large-scale, low surface brightness emission, provided by short baselines, but at the same time allowing an accurate subtraction of discrete sources, which are best identified by long baselines. This may be the reason for the relatively low number of mini-halos known – currently, about thirty mini-halos (or candidates) have been detected (e.g., Richard-Laferrière et al., 2020). In fact, although a correspondence between radio mini-halos and cool cores is well recognized, it is still not clear whether these radio sources are intrinsically common or rare in CC clusters. Studies of mass-selected sample of massive clusters ($M_{500} > 6 \times 10^{14}$ M$_\odot$ derived from Planck observations) found an occurrence of mini-halos as high as 80% (Giacintucci et al., 2017). However, larger statistical samples, that include lower-mass systems, are crucial to firmly establish the occurrence of mini-halos among the general CC population. Good cluster statistics in terms of X-ray properties are already currently available from *Chandra* and *XMM-Newton* and can be exploited to forecast future detection of radio mini-halos, provided that an intrinsic relation between the thermal and

non-thermal cluster properties exists. For this purpose, Gitti et al. (2015) and Gitti et al. (2018) investigated the link between global X-ray and radio observables that can be easily obtained from (present and future) cluster surveys, such as the luminosities. Since all known mini-halos are hosted by clusters with low central entropy (Hudson et al., 2010), the basic assumption is that every strong CC cluster hosts a radio mini-halo that follows the observed correlation between the 1.4 GHz radio power of the mini-halos, $P_{1.4}$, and the global X-ray luminosity of the host clusters, $L_{\rm X}$ (e.g., Cassano et al., 2008; Kale et al., 2013; Gitti et al., 2018; Giacintucci et al., 2019). This $P_{1.4}$-L_X correlation can we written in the form:

$$\log P_{1.4} = a \, \log L_{\rm X} + b, \tag{1}$$

where $P_{1.4}$ is in units of 10^{24} W/Hz and $L_{\rm X}$ is in units of 10^{44} erg/s.

In particular, Gitti et al. (2018) estimated the maximum number of radio mini-halo candidates that can potentially be discovered by the SKA-Mid and SKA-Low surveys as a function of redshift z. This was achieved by integrating the radio luminosity function (RLF) of mini-halos over radio luminosity and redshift, where the RLF of mini-halos is obtained from the X-ray luminosity function (XLF) of clusters[3] by considering the observed $P_{1.4}$-L_X correlation and the fraction of clusters with strong cool cores (~ 0.4, Hudson et al., 2010). This correlation indicates a connection between the energy reservoir in CC clusters and that associated with the non-thermal components powering radio mini-halos (see also Bravi et al., 2016). The non-thermal power, $P_{\rm NT}$, that can be sustained in the region of radio mini-halos over timescales longer than the radiative lifetime of relativistic electrons depends on the magnetic field strength as $P_{\rm NT} = P_{\rm radio} + P_{\rm IC} = P_{\rm radio}[1 + (B_{\rm CMB}/B_{\rm MH})^2]$, where $P_{\rm radio}$ is the synchrotron power, $P_{\rm IC}$ is the inverse Compton (IC) power, $B_{\rm CMB} = 3.25\,(1+z)^2\,\mu$G is the magnetic field equivalent to the inverse Compton losses with CMB photons, and $B_{\rm MH}$ is the average magnetic field intensity in the mini-halo region. The observed synchrotron radiation is thus a function of the intra-cluster magnetic field and redshift: $P_{\rm radio}(B_{\rm MH}, z) \propto B_{\rm MH}^2/[B_{\rm MH}^2 + B_{\rm CMB}^2(z)]$, where we made the dependencies explicit. Conversely, by normalizing the radio luminosity to the observed X-ray luminosity through the measured $P_{1.4}$-L_X correlation, the mini-halo RLF can be linked to the cluster XLF with a dependence on the parameters a, b (see Eq. 1) and magnetic field $B_{\rm MH}$, only. More details about this approach can be found in Gitti et al. (2018, and references therein).

In this chapter we update the previous work at mid frequencies by considering the $P_{1.4}$-L_X correlation derived from the mini-halo compilation of Richard-Laferrière et al. (2020), with $a = 1.97 \pm 0.31$ and $b = -1.72 \pm 0.31$ (see Fig. 2, left panel). We consider the radio observational performances of the full Design Baseline (Array Assembly 4, AA4) of the SKA-Mid telescope at Band 2 with rms of ~ 4 μJy/beam at $\sim 8''$ resolution (Briggs 0 image weighting and $\sim 4''$ tapering). According to the SKAO online sensitivity calculator[4], this sensitivity can be achieved with 10 minutes of on-source observing time, thus a survey as wide as an all-sky survey (3π sr) could be completed in about 7 months. The survey details are summarized in Table 1 (raw labeled "Mini-halos"). We note that this survey would also provide higher-resolution images ($< 1''$), which can be used to estimate and subtract the contribution of the BCG (raw labeled "(BCG subtract.)" in Table 1) from the extended

[3] We considered the evolving XLF derived from the high-redshift X-ray–selected 160 Square Degree *ROSAT* Cluster Survey (160SD) by Mullis et al. (2004) in a Λ-dominated universe.

[4] https://sensitivity-calculator.skao.int

radio emission. Our predictions are shown in the right panel of Fig. 2, where we plot the number of mini-halos expected to be observable in different redshift bins, assuming three reference values of $B_{\rm MH} = 1\,\mu$G (blue), 10 μG (black), and 30 μG (red). Despite the large error bars, we note that models with low and high magnetic field values yield different expectations at $z > 0.6$. Specifically, the predicted number of mini-halos is only a few for $B_{\rm MH} = 1\,\mu$G, and ≥ 20 for $B_{\rm MH} = 30\,\mu$G. This is primarily due to the fact that, in the presence of weak magnetic fields, an increasing fraction of the non-thermal luminosity is channeled into IC emission at higher redshifts. As a result, mini-halos become progressively fainter and more challenging to detect. Based on our estimates, upcoming SKA-Mid surveys will thus offer a mean to discriminate between different values of magnetic field strength in mini-halos.

We note that the predictions presented above for the AA4 SKA-Mid telescope, computed using the updated $P_{1.4}$–L_X correlation (Richard-Laferrière et al., 2020), are consistent with the results of Gitti et al. (2018), where the potential contributions from SKA-Low were also discussed. Accounting for the additional uncertainties in the spectral index when extrapolating to low frequencies, we therefore expect the predictions shown in Fig. 5 (bottom right panel) of Gitti et al. (2018) to be valid also for the AA4 SKA-Low telescope. In particular, an all-sky survey with SKA-Low may be able to detect up to 10^4 new mini-halos out to redshift $z \sim 1$, where a non-detection of mini-halos above $z \sim 0.6$ would indicate a low magnetic field value $B_{\rm MH} < 1\,\mu$G. We estimated that the observational performances adopted in that work (rms $\sim 20\,\mu$Jy/beam at $\sim 8''$ resolution, with Briggs 0 image weighting) can be achieved with 10 minutes of on-source observing time with the AA4 SKA-Low telescope, where higher resolution images ($\sim 3''$, with uniform weighting) can be used to account for the central BCG contribution. Considering the expected SKA-Low field of view (FOV ~ 7 deg^2 at the central frequency of 200 MHz), this survey could thus be completed in about 1 month.

2.3 Synergy with NewAthena: investigating the role of turbulent re-acceleration

The estimates presented in Sect. 2.2 assume that all CC clusters host a mini-halo, regardless of their mass or dynamical state. This may be reasonable within hadronic models, where the radio emissivity depends on the density of ICM thermal protons, but in re-acceleration or leptonic scenarios, sustaining radio-emitting electrons depends also on the turbulence level and the fraction of turbulent energy dissipated into particle re-acceleration. As discussed in Sect. 2.1, turbulence may be driven by the interplay between outflowing relativistic plasma from AGN jets and lobes, responsible for AGN feedback, and mild dynamical activity inducing motions of the ICM. If turbulence is triggered by core perturbations from large-scale dynamics (e.g., ZuHone et al., 2013), it is expected to weaken in less massive and less disturbed systems. This may reduce the occurrence of mini-halos in CC clusters, leading to a lower number density than predicted by simplified models. On the other hand, turbulence may be higher at high redshift where clusters are still forming (Hlavacek-Larrondo et al., 2025). Although this adds uncertainty to theoretical expectations, it underscores the importance of comparing them with future survey data. Such comparisons will help to constrain the role of turbulence and re-acceleration in mini-halos, and may clarify their physical origin. According to numerical simulations (ZuHone et al., 2013), turbulence with velocity broadening $\sigma_{\rm turb} \sim$ 50-200 km/s on spatial scales below ~50-100 kpc in the CC region is potentially sufficient to re-accelerate seed relativistic electrons producing radio mini-halos. Such turbulence levels are in the reach of the

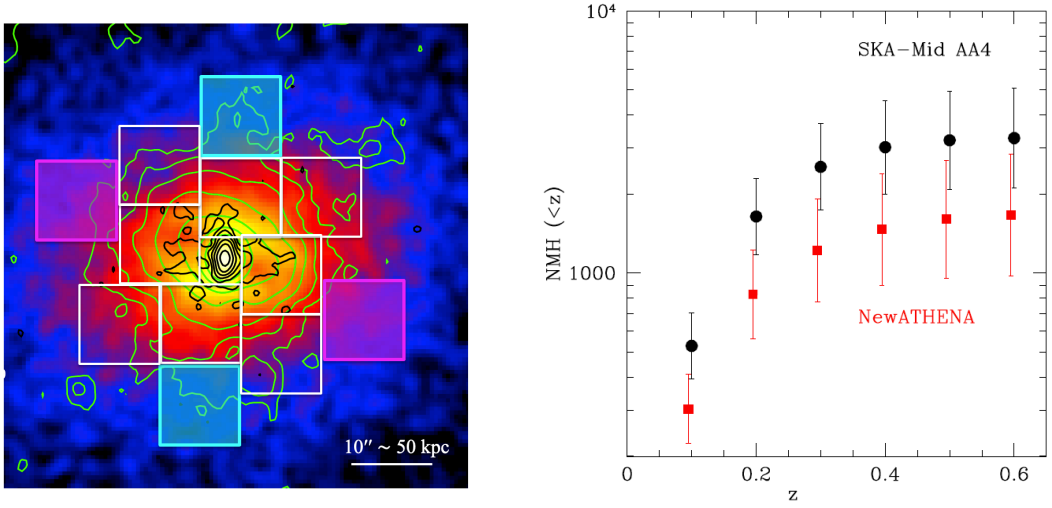

Figure 3: *Left panel: Chandra* image of the cluster RBS 797 (z=0.35, 1″ ~ 5 kpc) with the contours of the mini-halo radio emission (in green, starting at 0.035 mJy/beam and increasing by a factor of 2, beam ~ 3″, Doria et al., 2012) and radio-loud BCG (in black, starting at 0.03 mJy/beam and increasing by a factor of 2, beam ~1.3″, Gitti et al., 2013). Shown in white is an example of the mesh for the point-to-point analysis, where the side of the box regions is 10″, similar to the X-IFU pixel size. The shaded boxes are the ones we considered for a preliminary feasibility, with colors indicating the input value of the turbulent velocity broadening (cyan=70 km/s, magenta=120 km/s). By using the *Xspec* command `fakeit`, we simulated X-IFU spectra with an exposure of 2 Ms. *Right panel:* In black is shown the integral number of radio mini-halo candidates detectable in the all-sky (3π sr) survey by AA4 SKA-Mid at Band 2 (see Table 1) up to a certain redshift, estimated by assuming a reference value of $B_{\rm MH} = 10\,\mu$G (black). In red is shown the relative number of clusters that can be followed-up by *NewAthena* X-IFU with a point-to-point analysis measuring the turbulent velocity broadening in box regions (similar to the ones shown in the left panel), as described in the text. The error bars indicate the 1σ uncertainty driven by the $P_{1.4}$-$L_{\rm X}$ correlation (Eq. 1).

X-IFU instrument on board *NewAthena*[5], which is expected to resolve gas velocities of ~10 km/s in the cluster cores on ~9 arcsec scales[6] (Cruise et al., 2025).

Motivated by these considerations, we investigated the science capabilities possible with a synergy of SKA-Mid surveys and *NewAthena* to address the issue on the origin and role of turbulence in powering mini-halos. Point-to-point studies of the correlation between the radio and X-ray surface brightness have been proven to be important in investigating the origin of mini-halos (e.g., Ignesti et al., 2020). The step forward we propose here is to adopt a similar approach to investigate the point-to-point correlation between the non-thermal properties of mini-halos and the ICM turbulent motions. This is essential to investigate the turbulent re-acceleration scenario for the origin mini-halos, and to evaluate the role of AGN feedback in powering the mini-halo emission.

We performed a preliminary feasibility study with X-IFU in a medium-redshift cluster, which shows clear bipolar radio lobes filling prominent X-ray cavities embedded in a mini-halo (RBS 797 at z=0.35, Gitti et al., 2006, 2013; Doria et al., 2012; Ubertosi et al., 2021, see Figs. 1 and 3). In particular, we simulated 2 Ms spectra in four 10″ × 10″ box regions along the edge

[5] `http://www.the-athena-x-ray-observatory.eu/`, expected launch date in late 2030s.
[6] 9 arcsec corresponds to ~70 kpc at z~1.

of the halo emission (at radial distances $\sim 20''$), located in opposite directions so as to probe anisotropic Gaussian $\sigma_{\rm turb}$ for the turbulent velocity broadening (Fig. 3, left panel). By starting from the observed *Chandra* spectra, we derived the initial parameters of the spectral fit (temperature, abundance, normalization) and used these information to produce emission models which assume a turbulent velocity broadening with an anisotropic radial gradient, arbitrarily chosen to be higher along the AGN lobe direction as can be expected if the turbulence is induced by the AGN activity. Input values (consistent with observational measurements, e.g., XRISM Collaboration et al., 2025b) range from 120 km/s along the AGN lobe – X-ray cavity direction to 70 km/s along the edge of the mini-halo in the opposite direction (magenta boxes and cyan boxes, respectively, in Fig. 3, left panel). By performing several `Xspec` simulations, we found that velocity broadening differences of approximately 70 km/s between various radial directions can be detected at $\approx 4\sigma$ on scales of $\sim 10''$. With this kind of study, we will thus be able to derive not only a global level of turbulence in CC clusters, providing a basis for comparison with more massive and dynamically active systems, but also the local correlation between turbulent velocity broadening and the non-thermal properties of the mini-halo. This, in turn, will help pinpoint the role of turbulence and re-acceleration mechanisms in mini-halos, and may offer a pathway to distinguish between different physical origins of these radio sources.

We further estimated the integral number of clusters up to a certain redshift for which *NewAthena* can perform this kind of point-to-point analysis on SKA-detected mini-halo samples. This is shown in the right panel of Fig. 3 in comparison with the number of mini-halo candidates observable by SKA-Mid, assuming a reference magnetic field value of $B_{\rm MH} = 10\,\mu$G. In particular, all-sky surveys conducted with the AA4 SKA-Mid configuration would be able to detect up to ~3500 new mini-halos out to redshift $z \sim 0.6$ (and up to 10^4 with the SKA-Low, see Sect. 2.2), thus producing a breakthrough in the study of these sources. We estimated that *NewAthena* can, in principle, perform a detailed follow-up of more than 50% of SKA-detected mini-halos at any redshift, although each cluster would require a pointed exposure as we simulated. The best strategy will thus be to define well-selected, pilot sub-samples of mini-halo clusters (as done e.g., in Ignesti et al., 2020) to undertake this kind of investigation.

3 BCG radio properties and AGN feedback as a function of cosmic epoch

3.1 Tracing radio-mode feedback in cluster cores

The radio-mode feedback is expected to be efficient in any cool core, in order to prevent the formation of massive cooling flows and extreme star formation rates in the BCG (McNamara et al., 2006; Rafferty et al., 2008). The presence of a radio galaxy in the BCG of a cluster is predicted to be generally associated to radio bubbles (X-ray cavities) and shocks in the ICM (see Section 1). As cavities are easier to detect than shock fronts, and hundreds of groups and clusters with cavities are known (e.g., Shin et al., 2016; Olivares et al., 2022), they are routinely used as tracers of AGN heating. The enthalpy of the cavities ($4pV$ for relativistic plasma, where p is the pressure of the surrounding ICM and V is the cavity volume) is a proxy of the outburst energetics (Bîrzan et al., 2004; Bîrzan et al., 2008), which, in the few known cases of clusters with both cavities and shocks, has been shown to be comparable with the energetics of shock fronts (e.g., Ubertosi et al., 2023) and scales with the X-ray radiative losses of the ICM (e.g., Eckert et al., 2021). Radio BCGs are thus

critical to maintain the large-scale cooling and heating balance and efficiently quench star formation in cluster cores (Croton et al., 2006). This is true not only for the secular evolution of massive, virialized clusters; indeed, several strong radio sources are the beacon of massive protoclusters at redshift 2 and larger (see, e.g., Miley et al., 2006; Hatch et al., 2014; Chiaberge et al., 2010; Overzier, 2016; Tozzi et al., 2022; Travascio et al., 2025). Recently, medium-deep JVLA observations of the core of the Spiderweb protocluster in the S, X and Ka bands, showed in detail the interaction of powerful jets with the surrounding cold and hot medium (Carilli et al., 2022) and the ongoing magnetization process of the proto-ICM (Anderson et al., 2022).

Tracing the feedback in galaxy clusters in the radio band consists of detecting the presence of radio AGN in the central galaxy, measuring its total power and resolving the radio emission in the radio lobes filling the cavities and driving the shock fronts in the ICM. These studies have been very successful for local targets, where deep radio and X-ray data are both available, but they become increasingly difficult at higher redshifts. Recently, a few studies focused on high-redshift clusters and on the evolution of their properties with cosmic time. They show a lack of evolution in the fraction of clusters hosting cool cores (Andrade-Santos et al., 2017; Ruppin et al., 2021), ~40% for $z \leq 1.4$, and a similar stability over cosmic time in the fraction of clusters hosting cavities, ~10% for $z \leq 1.1$ (Hlavacek-Larrondo et al., 2015; Olivares et al., 2022). It has thus been realized that, at least out to z~1, the evolution of cool-cores mirrors the evolution of feedback. Additionally, Santos et al. (2010) showed that for low and medium redshift clusters, the radio galaxies in the center of cool-cores have radio powers ranging from $\sim 10^{23}$ W/Hz to 10^{25} W/Hz. Only a few programs have been carried out to target medium and high redshift clusters with deep, high resolution radio data to perform a systematic investigations of the radio-mode feedback up to z~1. Among these studies, the JVLA follow-up of CLASH (Postman et al., 2012) clusters (Yu et al., 2018), and the investigation of the radio properties of BCGs in X-ray selected galaxy clusters (Hogan et al., 2015), showed that ≥90% of BCGs in relaxed clusters have 1.4 GHz radio powers above 10^{23} W/Hz. In addition, high resolution X-ray data from *Chandra* enable the measurement of the low-level nuclear activity in the BCG, despite the overwhelming ICM emission, and, therefore, the investigation of the complex relationship between radio and X-ray nuclear power in BCGs (Russell et al., 2013; Yang et al., 2018).

Based on these considerations, we conclude that in order to trace radio-mode AGN feedback we need to detect every radio galaxy at least down to 10^{23} W/Hz (at 1.4 GHz) at high redshift. In Figure 4 we show the radio power in unresolved sources corresponding to a detection limit of 1 μJy (blue solid line). Assuming that typically a detection requires a signal to noise ratio $S/N \sim 5$, these values correspond to an rms noise of 0.2 μJy per beam, which can be achieved with 30 hours of on-source observing time with the AA4 SKA-Mid telescope at Band 2. This sensitivity is obtained at an angular resolution ~0.75″ (Briggs 0, no tapering), below confusion limit, and as Figure 4 demonstrates, it will allow a complete census of the radio properties of the BCG above 10^{23} W/Hz at 1.4 GHz up to redshift $z \sim 2$ (the largest redshift where virialized galaxy clusters are currently found). A Deep Tier survey over about 10-30 deg^2, as the reference survey discussed by Prandoni and Seymour (2015), could be completed in less than 2 months (see Table 1). Considering that on the entire sky there are potentially 4×10^4 massive clusters at $z > 0.5$ which are within the reach of

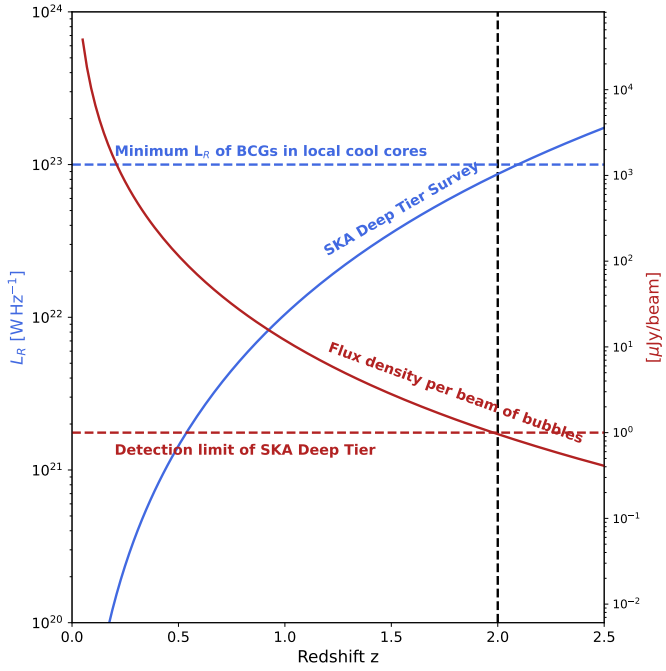

Figure 4: *Left y-axis (blue):* The blue solid line shows the 1.4 GHz luminosity corresponding to a detection limit of 1 Jy (defined as 5× rms noise), which will be reached by SKA-Mid Deep Tier surveys (see Tab. 1). The blue horizontal dashed line indicates the minimum luminosity currently measured in radio galaxies hosted in local CC clusters. *Right y-axis (red):* The red solid line shows the expected surface brightness with a resolution of 0.75″ for a bubble with radio power of ∼10^{24} W/Hz and physical size of ∼12 kpc, as in the reference cluster adopted in this work. The red horizontal dashed line marks the detection limit of the Deep Tier surveys with SKA-Mid at the same angular resolution. The vertical dashed black line indicates the highest redshift where virialized, X-ray emitting clusters have been detected.

NewAthena or *AXIS*[7] (Reynolds et al., 2024; Russell et al., 2024; Koss et al., 2025), the number of galaxies with radio activity in cool cores at $z > 0.5$ can be as high as $\sim 2 \times 10^4$, assuming little or no evolution in the population of CC clusters, or few thousands assuming a strong evolution by a factor of 10 (so-far ruled out at least up to z∼1, see Ruppin et al., 2021). Therefore, a strong synergy of the SKA with wide X-ray data will characterize the BCG in massive clusters with a cool core and feedback activity and constrain the duty cycle of radio galaxies in groups and clusters across the cosmic epochs.

3.2 Radio lobes, cavities and the energy budget of feedback

A further major breakthrough in the investigation of radio-mode AGN feedback at high redshift is the detection and characterization of the radio lobes produced by the relativistic electrons, which are responsible for carving the cavities in the ICM clearly observed in X-ray local clusters (see e.g., Timmerman et al., 2024, for a recent example). If we use as a reference the bubble size of RBS 797 (see Figure 1) we can directly compute the typical angular size of the bubbles as a function of the redshift. The average size for a single RBS 797's bubble, assuming a spherical shape, is 12 kpc. If we focus on targets at $z > 1$ the angular size corresponds to about 1.5″, with a weak dependence on the redshift. We conservatively assume that a beam FWHM of half the size of the bubble is sufficient to resolve it. Therefore, considering that the measured radio power at 1.4 GHz for a single cavity in RBS 797 is 10^{24} W/Hz (Gitti et al., 2006; Ubertosi et al., 2024a), we compute the radio flux density at 1.4 GHz from a single cavity as a function of redshift, assuming a beam FWHM of 0.75″. We show in Figure 4 that the signal from a single cavity (red solid line) is above the detection

[7] https://axis.umd.edu/, expected launch date in 2032.

limit (defined as 5× rms noise) of AA4 SKA-Mid surveys with rms of 0.2 μJy per beam (see Deep Tier survey in Table 1) up to $z \sim 2$. This indicates that the detection of AGN feedback signatures will rely on observations with the SKA telescopes, as the angular resolution of *NewAthena* (∼9″) is not sufficient to detect X-ray cavities at high redshift.

3.3 Jet reorientation

Ultimately, we consider the mechanism of jet reorientation and its relation to the distribution of feedback energy in cool cores. In some well-studied BCGs, dramatic misalignments between successive AGN outbursts have been reported. For example, in RBS 797, multiple AGN outbursts in different directions (up to 90° misalignments) point to repeated changes in jet orientation (Gitti et al., 2006; Ubertosi et al., 2021). Explaining how jets reorient remains a major challenge, partially because of the lack of large samples. Existing investigations of RBS 797 relied on multi-frequency data from e.g., JVLA and LOFAR (e.g., Gitti et al., 2013; Ubertosi et al., 2024a), to study the dynamics and timescales of jet activity (which requires data at ≥3 frequencies). About 5 μJy/beam sensitivity at >1 GHz with ≤ 1″ resolution was necessary to map the misaligned radio lobes. These requirements demonstrate why sample studies are difficult with current facilities. Yet systems like RBS 797 are not rare: ∼30% of radio BCGs exhibit ≥45° jet reorientation (Ubertosi et al., 2024a). Understanding this phenomenon is especially important for cool cores, where distributing feedback energy is essential to maintain thermal balance. Observations with SKA-Mid at Band 2 will reach an rms of ~ 1 μJy/beam at ∼0.5″ resolution (Briggs −1, no tapering) in 3 hours on source. Therefore, a Wide survey (10^3 square degrees, see Table 1) could be completed in about 4 months. Using the same formalism of Gitti et al. (2018), we expect $\sim 2 \times 10^3$ X-ray luminous clusters over this area for $z \leq 0.5$. Assuming a 40% fraction of cool cores (e.g., Ruppin et al., 2021) and a 20% fraction of cool cores with more than one pair of bubbles (e.g., Olivares et al., 2022), we will be able to study the relative inclination of successive radio lobes in about ∼200 systems. Adopting a 30% fraction of BCGs with ≥ 45° jet misalignments (see Ubertosi et al., 2024b), this implies $\gtrsim 60$ clusters with strongly misaligned outbursts to follow-up with SKA-Mid pointed observations. With its sensitivities of 1-2 μJy/beam in 1 hour at ≥1 GHz and resolutions down to 0.04″ (Braun et al., 2019), SKA-Mid will achieve, in just 1.5 hour per object (0.5 hour at three frequencies), the same level of detail that required 15 hours of JVLA time for RBS 797. This will enable a systematic exploration of jet reorientation in radio galaxies at the center of cool cores.

4 Summary and conclusions

We explored the potential of future radio surveys with the full Design Baseline AA4 SKA-Mid telescopes to study the evolution of CC clusters. An outline of the surveys considered in this work is presented in Table 1. Our predictions for radio mini-halos (Sect. 2.2), obtained by integrating the RLF of mini-halos derived from the XLF of CC clusters by adopting the observed $P_{1.4}$-L_X correlation, suggest that SKA-Mid could identify up to approximately 3500 mini-halo candidates out to $z \sim 1$, although this relies on the optimistic assumption that all CC clusters host mini-halos. If mini-halos originate from turbulent re-acceleration, their occurrence may decline in less massive or more distant clusters. Additionally, the synchrotron fraction of non-thermal emission decreases with redshift depending on the magnetic field strength, implying that SKA surveys could constrain the magnetic field properties via the evolving RLF of mini-halos. For instance, based on our

Table 1: Outline of the AA4 SKA-Mid surveys at Band 2 (central frequency ν = 1.3 GHz) considered in this work (with performances similar to the reference surveys described in Prandoni and Seymour, 2015). Column 1: Science drivers; column 2: survey tier; column 3: survey area in units of square degrees; column 4: on-source integration time in units of minutes; column 5: robustness of Briggs image weighting; column 6: tapering defined as arcsec in the image plane; column 7: continuum surface brightness sensitivity in units of μJy/beam; column 8: major and minor axis (FWHM) of the synthesized beam-size in units of arcsec; column 8: survey duration in units of months, considering the expected SKA-Mid FOV ($\sim$ 1 deg^2). All values are based on the current SKAO online sensitivity calculator for AA4 (https://sensitivity-calculator.skao.int).

Science	Tier	Area (deg^2)	time (min)	R	Taper ($''$)	rms (μJy/b)	beam ($''$)	duration (months)
Mini-halos	All-sky	31×10^3	10	0	4.275	4.14	7.98×6.95	~ 7
(BCG subtract.)	All-sky	31×10^3	10	0	no	2.80	0.81×0.69	~ 7
AGN feedback	Deep	10 - 30	1800	0	no	0.21	0.81×0.69	< 2
Jet reorientation	Wide	10^3	180	-1	no	1.11	0.48×0.43	~ 4

calculations, the SKA-Mid detection of more than 10 mini-halos at $z > 0.6$ would imply relatively strong magnetic fields ($B_{\rm MH} \geq$ 10-30 μG), whereas a non-detection at the same redshift would point to much weaker fields ($B_{\rm MH} < 1\,\mu$G). Possible challenges in the detection of radio mini-halos include contamination from bright point sources, especially central BCGs, and limitations in dynamic range. However, SKA's planned angular resolutions, along with the possibility to implement visibility-based subtraction techniques, should mitigate these issues.
We also highlighted the synergy between radio surveys and future X-ray missions (Sect. 2.3). Simulations indicate that turbulence with velocity broadening $\sigma_{\rm turb} \sim$ 50-200 km/s on $\lesssim$100 kpc scales can re-accelerate relativistic electrons and produce mini-halos. These turbulence levels are within reach of *NewAthena*'s X-IFU, which will allow a follow-up of > 50% of SKA-Mid samples up to $z \sim 1$ by detecting anisotropic turbulence down to tens of km/s on arcsecond scales.

Our feasibility study further showed that the radio-mode AGN feedback will be unveiled practically at any level in clusters up to $z \sim 2$, close to the maximum redshift where virialized clusters have been detected in the X-ray band so far (Sect. 3). When the SKAO will be fully operational, the knowledge of distant galaxy clusters will be largely but unpredictably changed. A large number of optically and IR selected clusters will be available thanks to the forthcoming surveys of the Euclid[8] satellite and of the Vera C. Rubin Observatory[9]. Thanks to the ICM X-ray characterization of the cluster cores achievable with the *NewAthena* mission, and potentially the *AXIS* telescope, these can be directly combined with the radio data to fully characterize jet-driven bubbles and feedback.

[8] http://sci.esa.int/euclid/.
[9] https://rubinobservatory.org/.

References

M. L. Ahnen, S. Ansoldi, L. A. Antonelli, and et al. , 589:A33, May 2016. doi: 10.1051/0004-6361/201527846.

M. G. Akritas and M. A. Bershady. , 470:706, Oct. 1996. doi: 10.1086/177901.

C. S. Anderson et al. , 937(1):45, Sept. 2022. doi: 10.3847/1538-4357/ac7ec0.

F. Andrade-Santos et al. , 843(1):76, July 2017. doi: 10.3847/1538-4357/aa7461.

S. Andreon et al. , 522(3):4301–4309, July 2023. doi: 10.1093/mnras/stad1270.

Y. Ascasibar and M. Markevitch. , 650:102–127, Oct. 2006. doi: 10.1086/506508.

P. N. Best et al. , 379:894–908, Aug. 2007. doi: 10.1111/j.1365-2966.2007.11937.x.

N. Biava et al. , 508(3):3995–4007, Dec. 2021. doi: 10.1093/mnras/stab2840.

N. Biava et al. , 686:A82, June 2024. doi: 10.1051/0004-6361/202348045.

L. Bîrzan et al. , 607:800–809, June 2004. doi: 10.1086/383519.

L. Bîrzan et al. , 686:859–880, Oct. 2008. doi: 10.1086/591416.

A. Bonafede et al. , 680:A5, Dec. 2023. doi: 10.1051/0004-6361/202347567.

R. Braun et al. *arXiv e-prints*, art. arXiv:1912.12699, Dec. 2019. doi: 10.48550/arXiv.1912.12699.

L. Bravi, M. Gitti, and G. Brunetti. , 455:L41–L45, Jan. 2016. doi: 10.1093/mnrasl/slv137.

G. Brunetti and T. W. Jones. *International Journal of Modern Physics D*, 23:1430007, Mar. 2014. doi: 10.1142/S0218271814300079.

J. O. Burns. , 99:14–30, Jan. 1990. doi: 10.1086/115307.

C. L. Carilli et al. , 928(1):59, Mar. 2022. doi: 10.3847/1538-4357/ac55a0.

R. Cassano, M. Gitti, and G. Brunetti. , 486:L31–L34, Aug. 2008. doi: 10.1051/0004-6361:200810179.

R. Cassano et al. In *Advancing Astrophysics with the SKA – II (AASKAII)*. 2026. arXiv search: Report number AASKAII/Cassano01.

M. Chiaberge et al. , 710:L107–L110, Feb. 2010. doi: 10.1088/2041-8205/710/2/L107.

D. J. Croton et al. , 365:11–28, Jan. 2006. doi: 10.1111/j.1365-2966.2005.09675.x.

M. Cruise et al. *Nature Astronomy*, 9:36–44, Jan. 2025. doi: 10.1038/s41550-024-02416-3.

T. J. Dennis and B. D. G. Chandran. , 622:205–216, Mar. 2005. doi: 10.1086/427424.

M. Donahue and G. M. Voit. , 973:1–109, Aug. 2022. doi: 10.1016/j.physrep.2022.04.005.

A. Doria et al. , 753:47, July 2012. doi: 10.1088/0004-637X/753/1/47.

R. J. H. Dunn and A. C. Fabian. , 373:959–971, Dec. 2006. doi: 10.1111/j.1365-2966.2006.11080.x.

D. Eckert et al. *Universe*, 7(5):142, May 2021. doi: 10.3390/universe7050142.

A. C. Fabian. , 32:277–318, 1994. doi: 10.1146/annurev.aa.32.090194.001425.

A. C. Fabian. , 50:455–489, Sept. 2012. doi: 10.1146/annurev-astro-081811-125521.

B. L. Fanaroff and J. M. Riley. , 167:31P–36P, May 1974.

L. Feretti, G. Giovannini, F. Govoni, and M. Murgia. , 20:54, May 2012. doi: 10.1007/s00159-012-0054-z.

Y. Fujita and Y. Ohira. , 746:53, Feb. 2012. doi: 10.1088/0004-637X/746/1/53.

Y. Fujita, T. Matsumoto, and K. Wada. *JKAS*, 37:571–574, Dec. 2004.

M. Gaspari, F. Brighenti, and P. Temi. , 424:190–209, July 2012. doi: 10.1111/j.1365-2966.2012.21183.x.

M. Gaspari, F. Brighenti, and M. Ruszkowski. *Astronomische Nachrichten*, 334(4-5):394, Apr. 2013. doi: 10.1002/asna.201211865.

S. Giacintucci et al. , 841:71, June 2017. doi: 10.3847/1538-4357/aa7069.

S. Giacintucci et al. , 880(2):70, Aug. 2019. doi: 10.3847/1538-4357/ab29f1.

M. Gitti, G. Brunetti, and G. Setti. , 386:456–463, May 2002. doi: 10.1051/0004-6361:20020284.

M. Gitti, G. Brunetti, L. Feretti, and G. Setti. , 417:1–11, Apr. 2004. doi: 10.1051/0004-6361:20031750.

M. Gitti, L. Feretti, and S. Schindler. , 448:853–860, Mar. 2006. doi: 10.1051/0004-6361:20053998.

M. Gitti, C. Ferrari, W. Domainko, and et al. , 470:L25–L28, Aug. 2007. doi: 10.1051/0004-6361:20077658.

M. Gitti, F. Brighenti, and B. R. McNamara. *Advances in Astronomy*, 2012:950641, 2012. doi: 10.1155/2012/950641.

M. Gitti et al. , 557:L14, Sept. 2013. doi: 10.1051/0004-6361/201322401.

M. Gitti, P. Tozzi, G. Brunetti, and et al. *PoS(AASKA14)076*, art. 76, 2015.

M. Gitti, G. Brunetti, R. Cassano, and S. Ettori. , 617:A11, Sept. 2018. doi: 10.1051/0004-6361/201832749.

N. A. Hatch et al. , 445(1):280–289, Nov. 2014. doi: 10.1093/mnras/stu1725.

S. Heinz and E. Churazov. , 634(2):L141–L144, Dec. 2005. doi: 10.1086/498301.

S. Heinz, M. Brüggen, A. Young, and E. Levesque. , 373:L65–L69, Nov. 2006. doi: 10.1111/j.1745-3933.2006.00243.x.

e. a. Hitomi Collaboration. , 535:117–121, July 2016. doi: 10.1038/nature18627.

e. a. Hitomi Collaboration. *ArXiv e-prints*, Nov. 2017.

J. Hlavacek-Larrondo et al. , 421:1360–1384, Apr. 2012. doi: 10.1111/j.1365-2966.2011.20405.x.

J. Hlavacek-Larrondo et al. , 805(1):35, May 2015. doi: 10.1088/0004-637X/805/1/35.

J. Hlavacek-Larrondo et al. , 898(2):L50, Aug. 2020. doi: 10.3847/2041-8213/ab9ca5.

J. Hlavacek-Larrondo et al. , 987(2):L40, July 2025. doi: 10.3847/2041-8213/add527.

M. T. Hogan et al. , 453(2):1201–1222, Oct. 2015. doi: 10.1093/mnras/stv1517.

D. S. Hudson, R. Mittal, T. H. Reiprich, and et al. , 513:A37, Apr. 2010. doi: 10.1051/0004-6361/200912377.

A. Ignesti, G. Brunetti, M. Gitti, and S. Giacintucci. , 640:A37, Aug. 2020. doi: 10.1051/0004-6361/201937207.

S. Jacob and C. Pfrommer. , 467:1478–1495, May 2017. doi: 10.1093/mnras/stx132.

R. Kale et al. , 557:A99, Sept. 2013. doi: 10.1051/0004-6361/201321515.

M. Koss et al. *arXiv e-prints*, art. arXiv:2511.00253, Oct. 2025. doi: 10.48550/arXiv.2511.00253.

M. Lepore et al. , 682:A186, Feb. 2024. doi: 10.1051/0004-6361/202347538.

G. Lusetti et al. , 683:A132, Mar. 2024. doi: 10.1051/0004-6361/202347635.

A. B. Mantz et al. , 496(2):1554–1564, Aug. 2020. doi: 10.1093/mnras/staa1581.

M. Markevitch and A. Vikhlinin. , 443:1–53, May 2007. doi: 10.1016/j.physrep.2007.01.001.

P. Mazzotta and S. Giacintucci. , 675:L9–L12, Mar. 2008. doi: 10.1086/529433.

M. McDonald et al. , 774:23, Sept. 2013. doi: 10.1088/0004-637X/774/1/23.

M. McDonald, M. Gaspari, B. R. McNamara, and G. R. Tremblay. , 858(1):45, May 2018. doi: 10.3847/1538-4357/aabace.

B. R. McNamara and P. E. J. Nulsen. , 45:117–175, Sept. 2007. doi: 10.1146/annurev.astro.45.051806.110625.

B. R. McNamara and P. E. J. Nulsen. *New Journal of Physics*, 14(5):055023, May 2012. doi: 10.1088/1367-2630/14/5/055023.

B. R. McNamara et al. , 648:164–175, Sept. 2006. doi: 10.1086/505859.

G. K. Miley et al. , 650:L29–L32, Oct. 2006. doi: 10.1086/508534.

R. Mittal, D. S. Hudson, T. H. Reiprich, and T. Clarke. , 501:835–850, July 2009. doi: 10.1051/0004-6361/200810836.

C. R. Mullis, A. Vikhlinin, J. P. Henry, and et al. , 607:175–189, May 2004. doi: 10.1086/383234.

P. E. J. Nulsen and B. R. McNamara. *Astronomische Nachrichten*, 334(4-5):386, Apr. 2013. doi: 10.1002/asna.201211863.

V. Olivares et al. , 516(1):L101–L106, Oct. 2022. doi: 10.1093/mnrasl/slac096.

R. A. Overzier. , 24(1):14, Nov. 2016. doi: 10.1007/s00159-016-0100-3.

J. R. Peterson and A. C. Fabian. , 427:1–39, Apr. 2006. doi: 10.1016/j.physrep.2005.12.007.

C. Pfrommer and T. A. Enßlin. , 413:17–36, Jan. 2004. doi: 10.1051/0004-6361:20031464.

C. Pinto et al. , 480(3):4113–4123, Nov. 2018. doi: 10.1093/mnras/sty2185.

M. Postman et al. , 199:25, Apr. 2012. doi: 10.1088/0067-0049/199/2/25.

I. Prandoni and N. Seymour. *PoS(AASKA14)067*, 2015.

D. A. Rafferty, B. R. McNamara, and P. E. J. Nulsen. , 687:899–918, Nov. 2008. doi: 10.1086/591240.

C. S. Reynolds et al. In J.-W. A. den Herder, S. Nikzad, and K. Nakazawa, editors, *Space Telescopes and Instrumentation 2024: Ultraviolet to Gamma Ray*, volume 13093 of *Society of Photo-Optical Instrumentation Engineers (SPIE) Conference Series*, page 1309328, Aug. 2024. doi: 10.1117/12.3022993.

A. Richard-Laferrière et al. , 499(2):2934–2958, Dec. 2020. doi: 10.1093/mnras/staa2877.

C. J. Riseley et al. , 512(3):4210–4230, May 2022. doi: 10.1093/mnras/stac672.

F. Ruppin et al. , 918(2):43, Sept. 2021. doi: 10.3847/1538-4357/ac0bba.

H. R. Russell et al. , 432(1):530–553, June 2013. doi: 10.1093/mnras/stt490.

H. R. Russell et al. *Universe*, 10(7):273, June 2024. doi: 10.3390/universe10070273.

J. S. Santos, P. Tozzi, P. Rosati, and H. Böhringer. , 521:A64, Oct. 2010. doi: 10.1051/0004-6361/201015208.

J. S. Santos et al. , 539:A105, Mar. 2012. doi: 10.1051/0004-6361/201118162.

F. Savini et al. , 622:A24, Feb. 2019. doi: 10.1051/0004-6361/201833882.

J. Shin, J.-H. Woo, and J. S. Mulchaey. , 227(2):31, Dec. 2016. doi: 10.3847/1538-4365/227/2/31.

M. W. Sommer et al. , 466(1):996–1009, Apr. 2017. doi: 10.1093/mnras/stw3015.

M. Sun. , 704:1586–1604, Oct. 2009. doi: 10.1088/0004-637X/704/2/1586.

R. Timmerman et al. , 687:A31, July 2024. doi: 10.1051/0004-6361/202347974.

P. Tozzi et al. , 799(1):93, Jan. 2015. doi: 10.1088/0004-637X/799/1/93.

P. Tozzi et al. , 667:A134, Nov. 2022. doi: 10.1051/0004-6361/202244337.

A. Travascio et al. *arXiv e-prints*, art. arXiv:2508.20074, Aug. 2025. doi: 10.48550/arXiv.2508.20074.

F. Ubertosi et al. , 923(2):L25, Dec. 2021. doi: 10.3847/2041-8213/ac374c.

F. Ubertosi et al. , 944(2):216, Feb. 2023. doi: 10.3847/1538-4357/acacf9.

F. Ubertosi et al. , 688:A86, Aug. 2024a. doi: 10.1051/0004-6361/202349011.

F. Ubertosi et al. , 961(1):134, Jan. 2024b. doi: 10.3847/1538-4357/ad11d8.

R. J. van Weeren et al. , 215(1):16, Feb. 2019. doi: 10.1007/s11214-019-0584-z.

R. J. van Weeren et al. , 692:A12, Dec. 2024. doi: 10.1051/0004-6361/202451618.

R. J. van Weeren et al. , 546(2):stag054, Feb. 2026. doi: 10.1093/mnras/stag054.

F. Vazza and G. Brunetti. *arXiv e-prints*, art. arXiv:2507.04727, July 2025. doi: 10.48550/arXiv.2507.04727.

XRISM Collaboration et al. *arXiv e-prints*, art. arXiv:2508.05067, Aug. 2025a. doi: 10.48550/arXiv.2508.05067.

XRISM Collaboration et al. *arXiv e-prints*, art. arXiv:2509.04421, Sept. 2025b. doi: 10.48550/arXiv.2509.04421.

XRISM Collaboration et al. , 982(1):L5, Mar. 2025c. doi: 10.3847/2041-8213/ada7cd.

XRISM Science Team. *arXiv e-prints*, art. arXiv:2202.05399, Feb. 2022. doi: 10.48550/arXiv.2202.05399.

L. Yang et al. , 859(1):65, May 2018. doi: 10.3847/1538-4357/aabfd7.

H. Yu et al. , 853(2):100, Feb. 2018. doi: 10.3847/1538-4357/aaa421.

F. Zandanel, C. Pfrommer, and F. Prada. , 438:124–144, Feb. 2014. doi: 10.1093/mnras/stt2250.

I. Zhuravleva, E. Churazov, A. A. Schekochihin, and et al. , 515:85–87, Nov. 2014. doi: 10.1038/nature13830.

I. Zhuravleva, E. Churazov, P. Arévalo, and et al. , 458:2902–2915, May 2016. doi: 10.1093/mnras/stw520.

J. A. Zuhone and E. Roediger. *Journal of Plasma Physics*, 82(3):535820301, June 2016. doi: 10.1017/S0022377816000544.

J. A. ZuHone, M. Markevitch, G. Brunetti, and S. Giacintucci. , 762:78, Jan. 2013. doi: 10.1088/0004-637X/762/2/78.